From Inverse Sandwich $Ta_2B_7^+$ and Ta_2B_8 to Spherical Trihedral $Ta_3B_{12}^-$: Prediction of The Smallest Metallo-Borospherene

Yu Zhang, Xiao-Yun Zhao, Miao Yan, and Si-Dian Li*

Supporting Information

Fig. S1 Low−lying isomers of $Ta_2B_7^+$ at PBE0, BP86, and CCSD(T) levels.

Fig. S2 Low−lying isomers of Ta_2B_8 at PBE0, BP86, and CCSD(T) levels.

Fig. S3 Optimized structures of the lowest−lying C_{2v} $Ta_3B_{10}^+$, C_s $Ta_3B_{10}^-$, and C_s $Ta_3B_{11}^-$ at PBE0 level.

Fig. S4 Low−lying isomers of $Ta_3B_{12}^-$ at PBE0, BP86, and CCSD(T) levels.

Fig. S5 Optimized structures of D_{3h} $V_3B_{12}^-$ and D_{3h} NbB_{12}^-.

Fig. S6 MD simulations of $Ta_2B_7^+$ (**1**), Ta_2B_8 (**2**), and $Ta_3B_{12}^-$ (**3**) at 1200 K, 700 K, and 1200 K.

Fig. S7 Delocalized σ− and π−CMOs of D_{6h} Ta_2B_6 and $Ta_2B_7^+$ (**1**)

Fig. S8 Ring current maps of (a) D_{7h} $Ta_2B_7^+$ (**1**), (b) D_{8h} Ta_2B_8 (**2**), and (c) D_{3h} $Ta_3B_{12}^-$ (**3**).

Fig. S9 Simulated IR, Raman, and UV−vis spectra of (a) $Ta_2B_7^+$ (**1**) and (b) Ta_2B_8 (**2**) at PBE0.

Table S1 Optimized coordinates of (a) D_{7h} $Ta_2B_7^+$ (**1**), (b) D_{8h} Ta_2B_8 (**2**), (c) D_{3h} $Ta_3B_{12}^-$ (**3**) at PBE0.

Table S2 Optimized structures and coordinates (in Å) of the second, third, and fourth lowest-lying isomers of $Ta_3B_{12}^-$ at PBE0//B/aug−cc−pVTZ/Ta/Stuttgart+2f1g level.

Fig. S1 Low−lying isomers of $Ta_2B_7^+$ at PBE0, BP86 (in parentheses), and CCSD(T) (in square brackets) levels, with the relative energies indicated in eV.

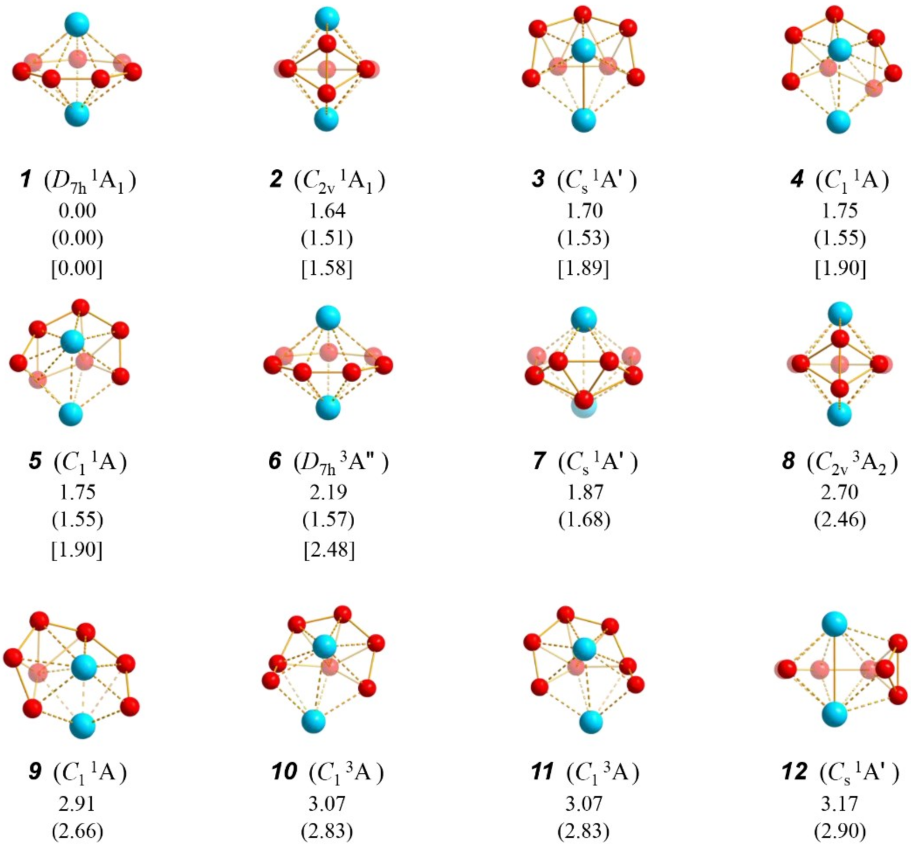

ΔE PBE0 B/ aug-cc-pVTZ/Ta/Stuttgart(2f1g) , () at BP86 B/aug-cc-pVTZ/ Ta/Stuttgart(2f1g) , [ ] at CCSD(T) B/aug-cc-pVTZ/ Ta/Stuttgart(2f1g)

Fig. S2 Low−lying isomers of Ta_2B_8 at PBE0, BP86 (in parentheses), and CCSD(T) (in square brackets) levels, with the relative energies indicated in eV.

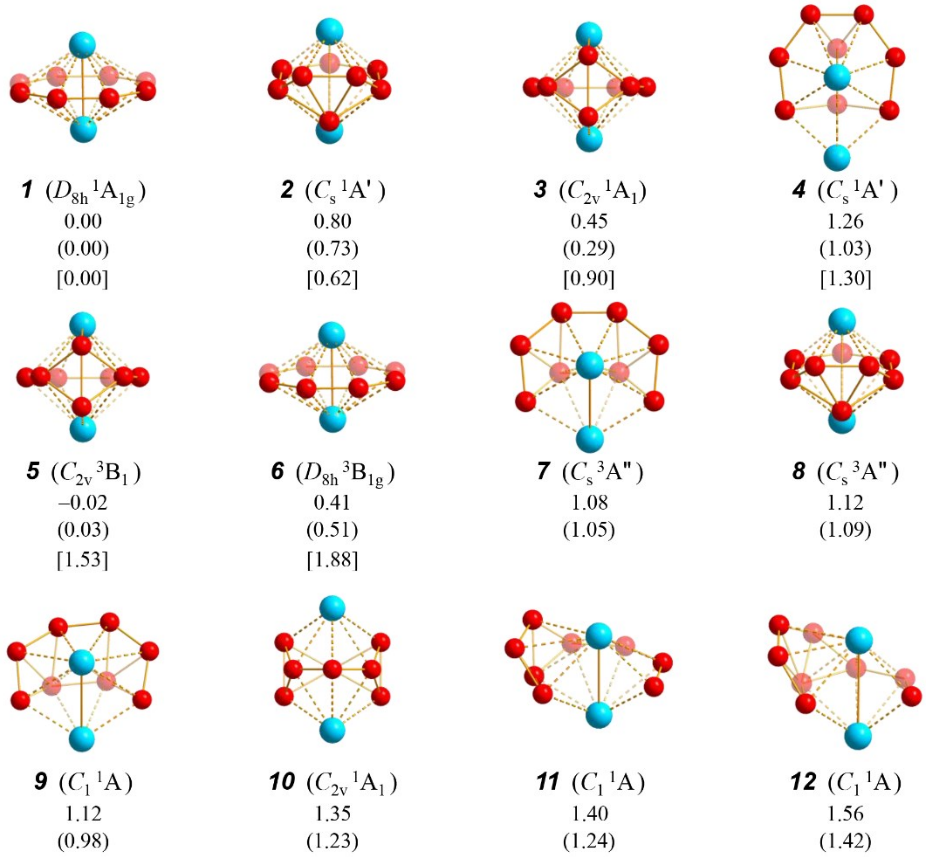

ΔE PBE0 B/ aug-cc-pVTZ/Ta/Stuttgart(2f1g) , () at BP86 B/aug-cc-pVTZ/ Ta/Stuttgart(2f1g) , [ ] at CCSD(T) B/aug-cc-pVTZ/ Ta/Stuttgart(2f1g)

Fig. S3 Optimized structures of the lowest−lying C_{2v} $Ta_3B_{10}^+$, C_s $Ta_3B_{10}^-$, and C_s $Ta_3B_{11}^-$ at PBE0//B/aug−cc−pVTZ/Ta/Stuttgart+2f1g level.

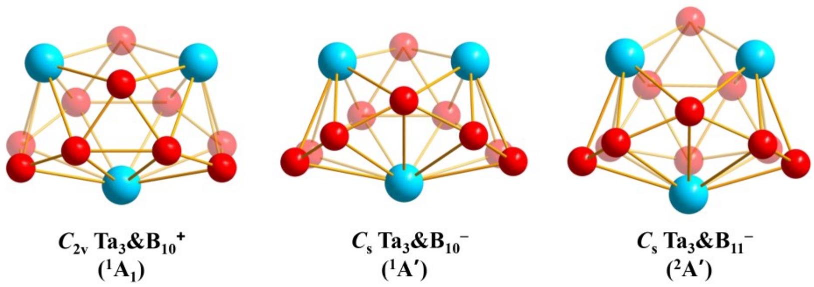

Fig. S4 Low−lying isomers of $Ta_3B_{12}^-$ at PBE0, BP86 (in parentheses), and CCSD(T) (in square brackets) levels, with the relative energies indicated in eV.

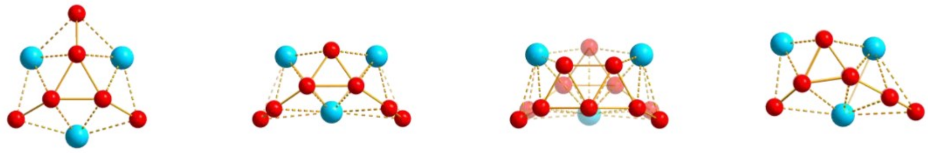

1 (D_{3h} $^1A_1'$)	***2*** (C_{2v} $^1A_1$)	***3*** (C_s $^1A'$)	***4*** (C_s $^1A'$)
0.00	−0.10	0.84	0.71
(0.00)	(−0.29)	(0.60)	(0.30)
[0.00]	[0.24]	[1.06]	[1.12]

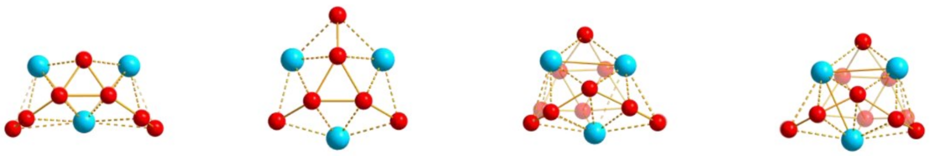

5 (C_{2v} $^3B_2$)	***6*** (C_{2v} $^3B_1$)	***7*** (C_1 ^1A)	***8*** (C_1 ^1A)
0.52	0.82	0.88	0.88
(0.29)	(0.73)	(0.57)	(0.57)

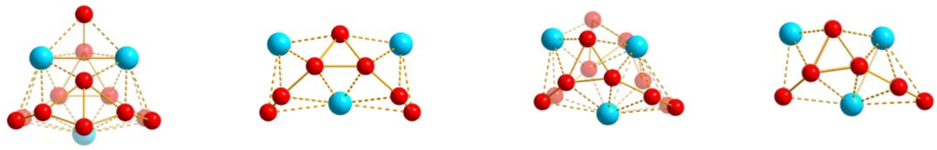

9 (C_s $^1A'$)	***10*** (C_{2v} $^3B_2$)	***11*** (C_1 ^3A)	***12*** (C_s $^3A'$)
0.87	1.11	1.30	1.75
(0.65)	(0.89)	(0.94)	(0.96)

ΔE PBE0 B/ aug-cc-pVTZ/Ta/Stuttgart(2f1g) , () at BP86 B/aug-cc-pVTZ/ Ta/Stuttgart(2f1g) , [ ] at CCSD(T) B/aug-cc-pVTZ/ Ta/Stuttgart(2f1g)

Fig. S5 Optimized structures of D_{3h} $V_3B_{12}^-$ and D_{3h} $Nb_3B_{12}^-$.

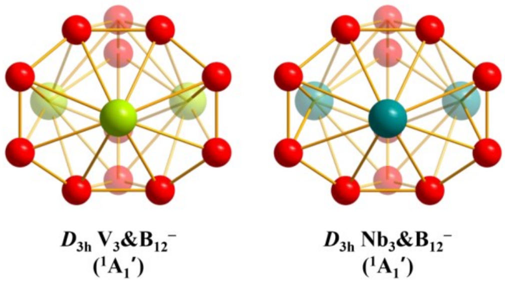

Fig. S6 MD simulations of $Ta_2B_7^+$ (**1**), Ta_2B_8 (**2**), and $Ta_3B_{12}^-$ (**3**) at 1200 K, 700 K, and 1200 K, respectively, with the calculated average root−mean−square−deviations (RMSD) and maximum bond length deviations (MAXD) indicated.

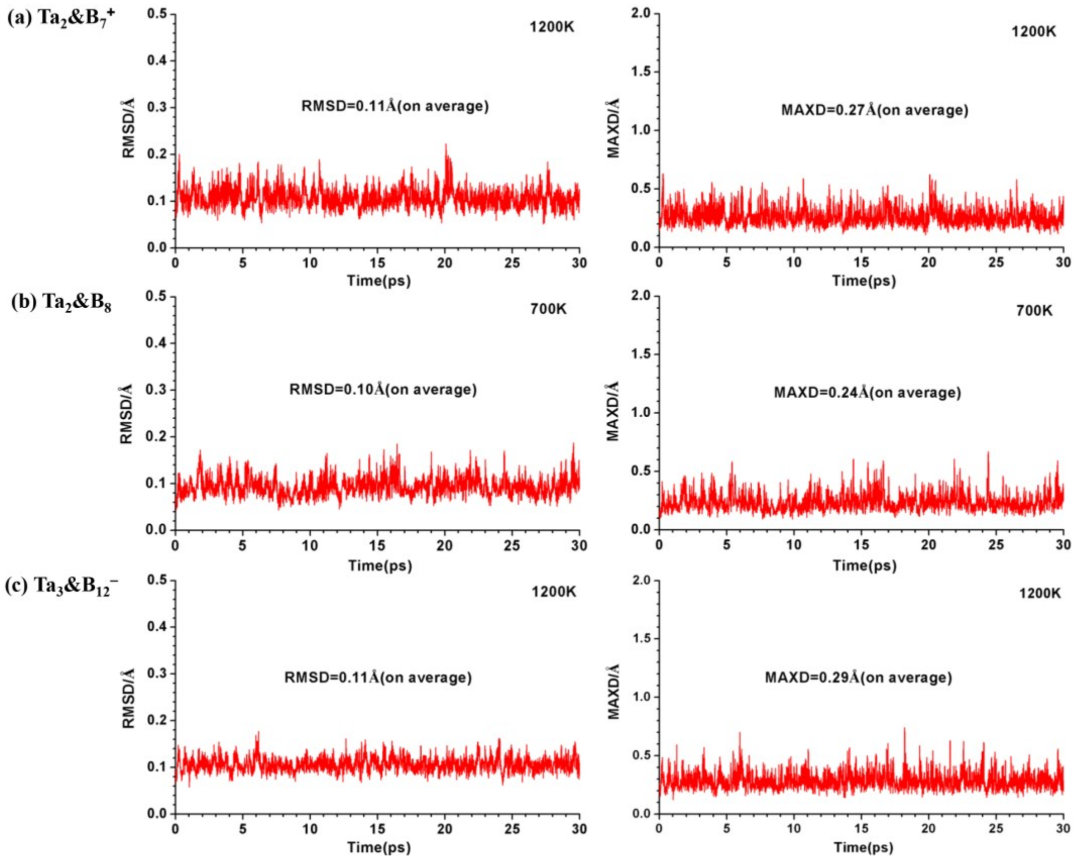

Fig. S7 Delocalized σ− and π−CMOs of (a) D_{6h} Ta_2B_6 and (b) $Ta_2B_7^+$ (**1**) at PBE0//B/aug−cc−pVTZ/Ta/Stuttgart+2f1g level.

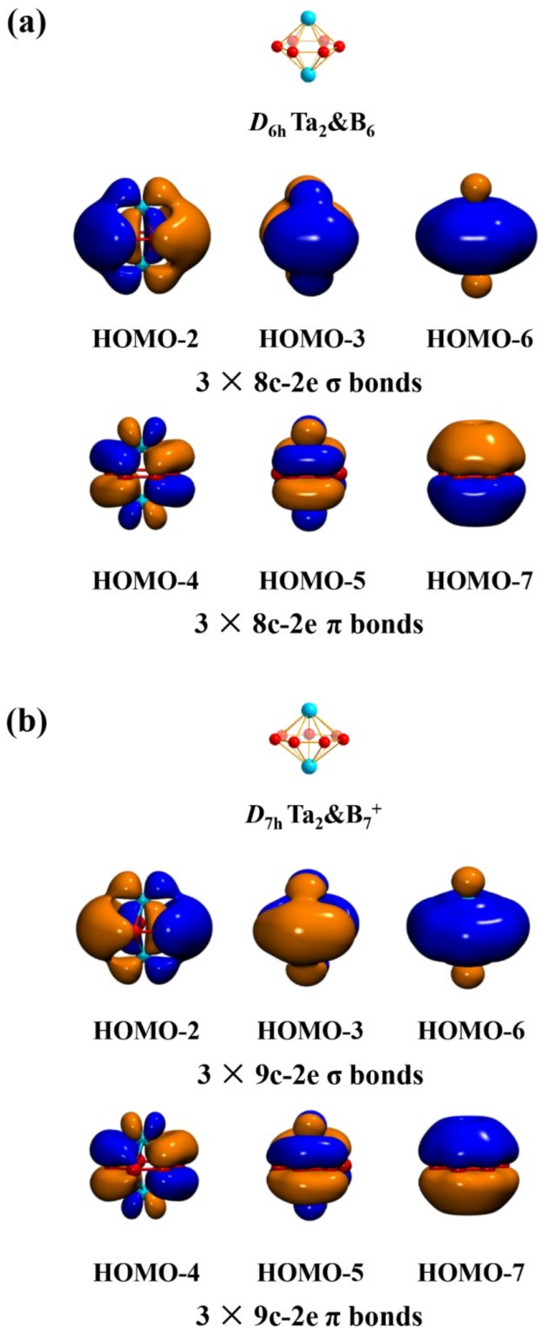

Fig. S8 Top and side views of the ring current maps of (a) D_{7h} $Ta_2B_7^+$ (**1**), (b) D_{8h} Ta_2B_8 (**2**), and (c) D_{3h} $Ta_3B_{12}^-$ (**3**) with the iso−surface value of 0.05. The external magnetic field B is applied in the vertical direction parallel to the C_7 axis of $Ta_2B_7^+$ (**1**), C_8 axis of Ta_2B_8 (**2**), and C_2 axis of $Ta_3B_{12}^-$ (**3**), with the induced current vectors represented by red arrows on the iso−surfaces.

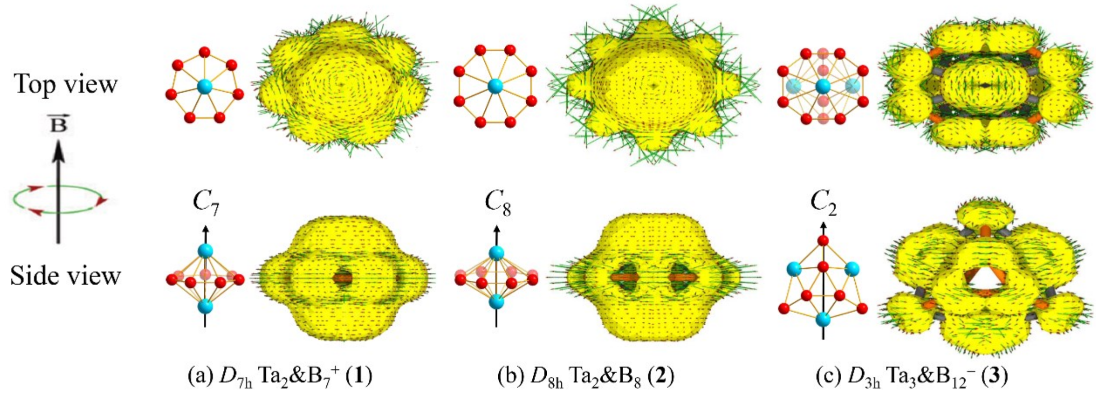

Fig. S9 Simulated IR, Raman, and UV−vis spectra of (a) $Ta_2B_7^+$ (**1**) and (b) Ta_2B_8 (**2**) at PBE0//B/aug−cc−pVTZ/Ta/Stuttgart+2f1g level.

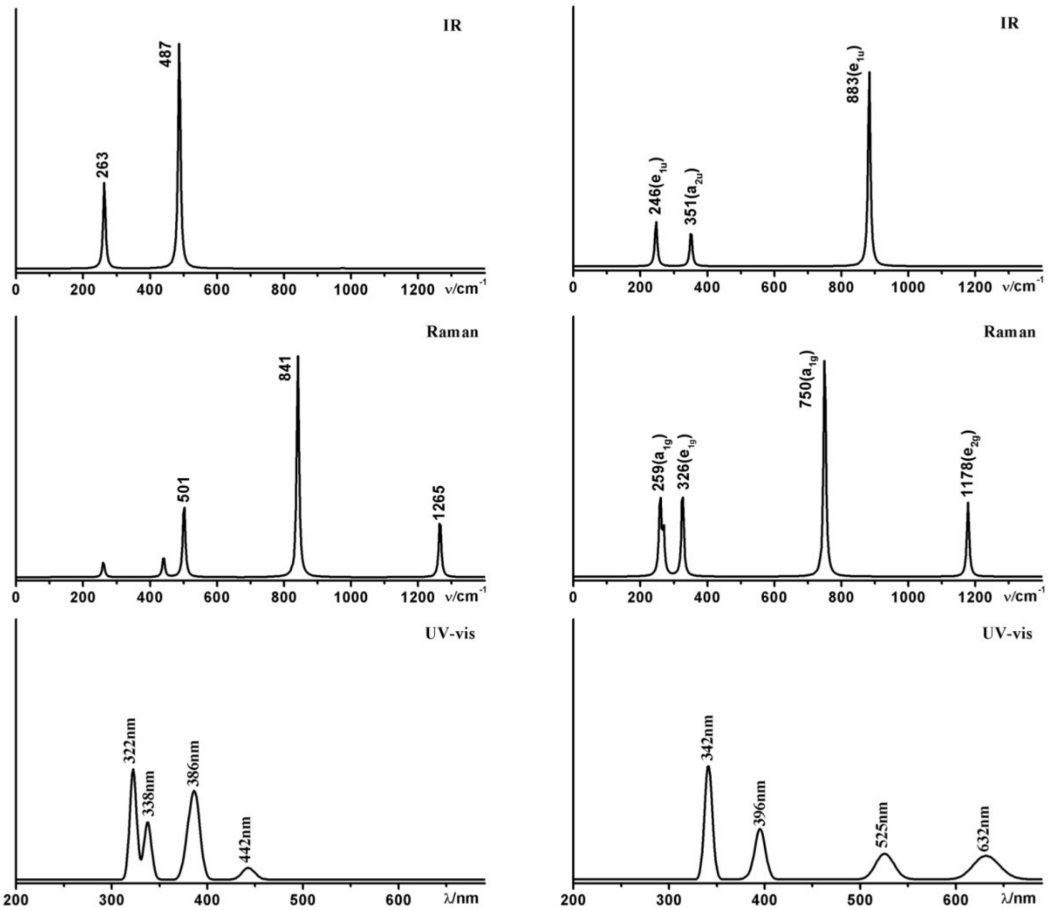

(a) D_{7h} Ta_2&B_7^+ (**1**)   (b) D_{8h} Ta_2&B_8 (**2**)

Table S1 Optimized coordinates (in Å) of (a) D_{7h} $Ta_2B_7^+$ (**1**), (b) D_{8h} Ta_2B_8 (**2**), and (c) D_{3h} $Ta_3B_{12}^-$ (**3**) at PBE0//B/aug–cc–pVTZ/Ta/Stuttgart+2f1g level.

(a) D_{7h} $Ta_2B_7^+$ (**1**)

B	0.00000000	1.77240700	0.00000000
B	1.38572300	1.10507800	0.00000000
B	1.72796900	-0.39439800	0.00000000
B	0.76901900	-1.59688300	0.00000000
B	-0.76901900	-1.59688300	0.00000000
B	-1.72796900	-0.39439800	0.00000000
B	-1.38572300	1.10507800	0.00000000
Ta	0.00000000	0.00000000	1.43155300
Ta	0.00000000	0.00000000	-1.43155300

(b) D_{8h} Ta_2B_8 (**2**)

B	0.00000000	2.01204000	0.00000000
B	-1.42272700	1.42272700	0.00000000
B	1.42272700	1.42272700	0.00000000
B	-2.01204000	0.00000000	0.00000000
B	0.00000000	-2.01204000	0.00000000
B	2.01204000	0.00000000	0.00000000
B	-1.42272700	-1.42272700	0.00000000
B	1.42272700	-1.42272700	0.00000000
Ta	0.00000000	0.00000000	1.26069100
Ta	0.00000000	0.00000000	-1.26069100

(c) D_{3h} $Ta_3B_{12}^-$ (**3**)

Ta	0.00000000	1.75299000	0.00000000
Ta	-1.51813400	-0.87649500	0.00000000
B	-0.86896500	0.50169700	1.66873400
B	-2.04920100	1.18310700	-0.79218300
B	2.04920100	1.18310700	0.79218300
B	0.00000000	-2.36621400	-0.79218300
B	-0.86896500	0.50169700	-1.66873400
Ta	1.51813400	-0.87649500	0.00000000
B	-2.04920100	1.18310700	0.79218300
B	0.86896500	0.50169700	-1.66873400
B	2.04920100	1.18310700	-0.79218300
B	0.00000000	-1.00339400	1.66873400
B	0.86896500	0.50169700	1.66873400
B	0.00000000	-1.00339400	-1.66873400
B	0.00000000	-2.36621400	0.79218300

Table S2 Optimized structures and coordinates (in Å) of the second (a), third (b), and fourth (c) lowest-lying isomers of $Ta_3B_{12}^-$ at PBE0//B/aug−cc−pVTZ/Ta/Stuttgart+2f1g level.

(a) C_{2v} $Ta_3\&B_{12}^-$ ($^1A_1$)

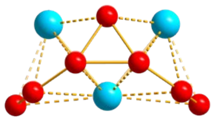

Ta	0.00000000	-0.00000000	-1.18138959
Ta	1.61200407	-0.00000000	0.79548931
B	-0.87388535	2.05490675	-0.24101743
B	0.87388535	2.05490675	-0.24101743
B	2.04989728	1.41510588	-1.05430960
B	-2.04989728	1.41510588	-1.05430960
B	-0.87388535	-2.05490675	-0.24101743
B	2.04989728	-1.41510588	-1.05430960
B	2.52818198	-0.00000000	-1.42127888
Ta	-1.61200407	-0.00000000	0.79548931
B	0.00000000	1.50686895	1.02193303
B	0.87388535	-2.05490675	-0.24101743
B	-2.04989728	-1.41510588	-1.05430960
B	0.00000000	-1.50686895	1.02193303
B	-2.52818198	-0.00000000	-1.42127888

(b) C_s $Ta_3\&B_{12}^-$ ($^1A'$)

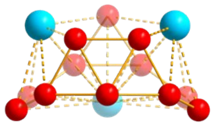

B	-1.97828846	0.00902592	-0.87616371
B	1.47502860	-1.16386702	-1.62116014
B	-1.24711597	1.20470515	0.00000000
B	0.07624476	-1.39914596	-2.37875132
B	-1.97828846	0.00902592	0.87616371
B	-1.36473271	-0.90129011	-2.05961627
B	2.08867015	-1.23110912	0.00000000
B	1.92055198	0.23141641	-0.83424377
B	1.47502860	-1.16386702	1.62116014
B	1.92055198	0.23141641	0.83424377
B	0.07624476	-1.39914596	2.37875132
B	-1.36473271	-0.90129011	2.05961627
Ta	0.05413926	0.80620507	-1.76350194
Ta	0.05413926	0.80620507	1.76350194
Ta	-0.18356362	-1.16897688	0.00000000

(c) C_s $Ta_3\&B_{12}^-$ ($^1A'$)

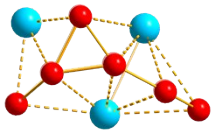

B	-0.90132581	0.74945409	-1.77220111
B	-0.77430741	-0.90645969	-1.56299986
B	0.51482107	-0.08179237	-2.16804413
B	2.01447036	0.06524607	-1.90556231
B	3.00927217	0.18263596	-0.75456444
B	3.00927217	0.18263596	0.75456444
B	2.01447036	0.06524607	1.90556231
B	0.51482107	-0.08179237	2.16804413
B	-0.77430741	-0.90645969	1.56299986
B	-0.90132581	0.74945409	1.77220111
B	-1.45299833	1.84115969	0.77559177
B	-1.45299833	1.84115969	-0.77559177
Ta	0.78855315	1.21481144	0.00000000
Ta	0.89842378	-1.24995120	0.00000000
Ta	-2.01710461	-0.21831828	0.00000000